Mukoyoshi *et al. Earth, Planets and Space* (2018) 70:36
https://doi.org/10.1186/s40623-018-0810-z

Earth, Planets and Space

FULL PAPER

Open Access

Slip parameters on major thrusts at a convergent plate boundary: regional heterogeneity of potential slip distance at the shallow portion of the subducting plate

Hideki Mukoyoshi[1*], Shunya Kaneki[2] and Tetsuro Hirono[2]

Abstract

Understanding variations of slip distance along major thrust systems at convergent margins is an important issue for evaluation of near-trench slip and the potential generation of large tsunamis. We derived quantitative estimates of slip along ancient subduction fault systems by using the maturity of carbonaceous material (CM) of discrete slip zones as a proxy for temperature. We first obtained the Raman spectra of CM in ultracataclasite and pseudotachylyte layers in discrete slip zones at depths below the seafloor of 1–4 km and 2.5–5.5 km, respectively. By comparing the area-under-the-peak ratios of graphitic and disordered bands in those Raman spectra with spectra of experimentally heated CM from surrounding rocks, we determined that the ultracataclasite and pseudotachylyte layers had been heated to temperatures of up to 700 and 1300 °C, respectively. Numerical simulation of the thermal history of CM extracted from rocks near the two slip zones, taking into consideration these temperature constraints, indicated that slip distances in the ultracataclasite and pseudotachylyte layers were more than 3 and 7 m, respectively. Thus, potential distance of coseismic slip along the subduction-zone fault system could have regional variations even at shallow depth ($\leq$ 5.5 km). The slip distances we determined probably represent minimum slips for subduction-zone thrusts and thus provide an important contribution to earthquake preparedness plans in coastal areas facing the Nankai and Sagami Troughs.

Keywords: Carbonaceous material, Raman spectroscopy, Frictional heating, Earthquake slip

Introduction

In a worldwide context, most of the seismic energy released by large earthquakes occurs in plate-subduction zones (Scholz 2002). Complex plate-boundary megathrusts, décollements, megasplay faults, and other types of thrust are known at many plate margins, including the Nankai Trough (Park et al. 2002; Moore et al. 2007; Tsuji et al. 2015) and the Alaskan (Plafker 1972) and Sunda margins (Kopp and Kukowski 2003). Fault systems such as these can generate very large tsunamis during great earthquakes such as the 1944 Tonankai earthquake (Park et al. 2002; Baba et al. 2006) and the 2011 Tohoku-oki earthquake (Yue and Lay 2011; Ito et al. 2011; Fulton et al. 2013). Notably, coseismic displacement of the seafloor exceeded 50 m at the trench axis during the 2011 Tohoku-oki earthquake (Ito et al. 2011; Kodaira et al. 2012; Sun et al. 2017).

To investigate the mechanism of gigantic seismic slip along the plate interface during the 2011 Tohoku-oki earthquake, Hirono et al. (2016) undertook quantitative laboratory analyses of the properties of plate-interface material retrieved during the Japan Trench Fast Drilling Project (JFAST) and ran simulations of fault weakening and rupture propagation. Their results indicated a large stress drop and slip of about 75 m near the trench during

*Correspondence: mukoyoshi@riko.shimane-u.ac.jp
[1] Department of Geoscience, Interdisciplinary Graduate School of Science and Engineering, Shimane University, Nishikawatsu-cho 1060, Matsue, Shimane 690-8504, Japan
Full list of author information is available at the end of the article

the earthquake, which is consistent with the amount of slip estimated from observations and surveys (50–80 m slip) (Fujiwara et al. 2011; Ito et al. 2011; Yue and Lay 2011; Sun et al. 2017). Although the style of deformation of sediments in the incoming plate could change with subducting regions during the subduction–accretion process, which was examined by analyzing mineral veins distributed in an ancient plate-subduction fault (Mukoyoshi et al. 2009), Hirono et al. (2016) did not consider the heterogeneity of fault-plane material at different plate subducting segments. Thus, in this study we focused on the slip parameters of the subduction fault system taking into consideration the regional heterogeneity of the plate-subduction faults.

To estimate slip parameters such as shear stress and slip distance, information about frictional heat within the slip zone is of paramount importance. Various temperature proxies have been proposed, including the thermomagnetic characteristics of magnetic minerals (Mishima et al. 2009; Chou et al. 2012), fluid-mobile trace element and isotope anomalies (Ishikawa et al. 2008; Honda et al. 2011), clay mineral dehydroxylation (Hirono et al. 2008a; Kuo et al. 2009), vitrinite reflectance (O'Hara 2004; Sakaguchi et al. 2007, 2011; Kitamura et al. 2012; Maekawa et al. 2014), and infrared and Raman spectroscopic characteristics of carbonaceous material (Hirono et al. 2015; Kaneki et al. 2016). Carbonaceous materials, including vitrinite, are commonly included within accretionary complexes in both intact sedimentary rocks and fault-zone rocks (e.g., Sakaguchi et al. 2007, 2011). A new method to investigate the thermal history of rocks by applying Raman spectroscopy to CM in conjunction with heating experiments has been proposed by Kaneki et al. (2016).

In this study, we examined discrete slip zones at 1–4 km depth within a major thrust and at 2.5–5.5 km depth within an ancient megasplay fault. We examined the microstructures of both CM-bearing fault zones and used Raman spectroscopy on CM to estimate the minimum temperatures to which they had been exposed. We determined slip distances by conducting numerical simulation and considered the differences of slip behavior along two different plate interfaces and its potential to trigger large tsunamis.

Geological setting

Accretionary complexes of Cretaceous to present age are distributed around the Pacific Ocean and are commonly divided into prisms of Cretaceous–Paleogene and Neogene–present age (Fig. 1a). These complexes were formed by subduction-related accretion in the Nankai and Sagami Troughs. For our study, we chose two Japanese locations where subducting strata within the incoming plate are at different depths of burial, one on the Boso Peninsula on Honshu Island and the other in the Shimanto accretionary complex on Shikoku Island.

On the Boso Peninsula, the Emi Group was defined by Kawai (1957), but has since been included in the Hota Group (Mitsunashi et al. 1979; Chiyonobu et al. 2017). The Emi Group is composed of late Oligocene to middle Miocene tuffaceous clastic sedimentary rocks (Sawamura and Nakajima 1980; Ogawa and Ishimaru 1991; Suzuki et al. 1996) and forms a fold-and-thrust system (Fig. 1b). The thermal history of the Emi Group, reconstructed from vitrinite reflectance data, indicates that it has been heated to temperatures of 50–75 °C (Hirono 2005) at an estimated maximum burial depth of 1–4 km below the seafloor (Hirono et al. 2008b). It contains a major east–west-striking back thrust, 5–10 mm thick, which includes a discrete slip zone composed of glossy black material accompanied by well-developed slickensides (Emi major thrust hereafter) (Fig. 2a).

In the Shimanto accretionary complex (Fig. 1c), there are several out-of-sequence thrusts (OST) in and around the Cretaceous Nonokawa Formation and Kure Mélange. The deformed zone (~500 mm thick) of a representative OST comprises an outer fracture-damaged zone, a cataclasite layer, and a narrow, black slip zone 0.5–5 mm thick (Kure OST hereafter) (Fig. 2b). The hanging wall of the Kure OST is composed of greenish shale, and the footwall is composed of sandstone. The depth below seafloor of the slip zone has been estimated from vitrinite reflectance data to be 2.5–5.5 km (Mukoyoshi et al. 2006).

Methods

We collected rock samples from outcrops of the surrounding rocks from which we extracted CM for heating experiments and Raman spectroscopic analysis. Rock samples of surrounding rocks were first crushed with a mortar and pestle and sieved to obtain 150–710 μm fragments. The CM, including vitrinite, and rock fragments were then separated using a sodium polytungstate solution (specific gravity, 1.8). The CM fragments were dried at 30 °C for > 24 h before the heating experiments. The concentration of CMs in the surrounding rocks was approximately 30 wt%. We also prepared thin sections of rock samples of the slip zones oriented perpendicular to the fault surface and parallel to the fault striations for Raman spectroscopic analysis.

To replicate the heating caused by earthquake slip, we heated the CM retrieved from the host rocks in a thermogravimetric apparatus (Netzsch STA 449 C Jupiter balance) to temperatures from 100 to 1300 °C, at increments of 100 °C, in an Ar gas atmosphere. Although the rate of temperature increase on the fault plane during an earthquake is several tens to several hundreds of degrees

per second (e.g., Lachenbruch 1986), we heated our samples at 50 °C min^{-1} because of the limited available heating rates of the apparatus.

Raman spectroscopy is widely used for analyses of CM. Recent progress in the use of Raman spectroscopy has been well reviewed by Potgieter-Vermaak et al. (2010). Typical spectra of CM contain several bands, the most intense being the first-order graphite (G) band that peaks at 1600 cm^{-1} and the defect (or disorder; D) band that peaks at 1350 cm^{-1}. The G band is attributed to the E_{2g} vibrational mode (representing a polyaromatic structure) with D^4_{6h} crystal symmetry, and is present in all CM, regardless of the degree of structural order (Tuinstra and Koenig 1970). The D band is assigned to the A_{1g} mode and is absent in perfectly stacked graphite but is induced by structural defects in CM (Tuinstra and Koenig 1970; Bény-Bassez and Rouzaud 1985). Poorly organized CM contains additional bands at about 1200 cm^{-1} (known as the D4 band), 1500 cm^{-1} (D3 band), and 1620 cm^{-1} (D2 band) (Beyssac et al. 2002, 2003; Sadezky et al. 2005; Guedes et al. 2010; Lahfid et al. 2010). The D4 band is attributed to either the sp^2–sp^3 bond or to C–C and C=C stretching vibrations in polyene-like structures (Dippel et al. 1999). The D3 band is attributed to out-of-plane defects, such as tetrahedral carbons; such defects are most likely released during the early stages of graphitization (Bény-Bassez and Rouzaud 1985). The D2 band forms a shoulder on the G band, but its significance is poorly understood. In very poorly organized CM, which was the case for all of our samples, the G and D2 bands cannot be resolved, so a single broad band occurs at around 1600 cm^{-1} (Beyssac et al. 2003). Although some studies have adopted a complicated waveform separation of four sub-peaks at around 1350–1700 cm^{-1} (e.g., Beyssac et al. 2002), the attribution of the sub-peaks at molecular level is not based on a complete understanding of the physicochemistry of CM. Therefore, we used only the D and G bands for our spectroscopic analysis.

We used a Raman microspectrometer equipped with a 532-nm laser (XploRA; HORIBA Jobin–Yvon Inc.) to

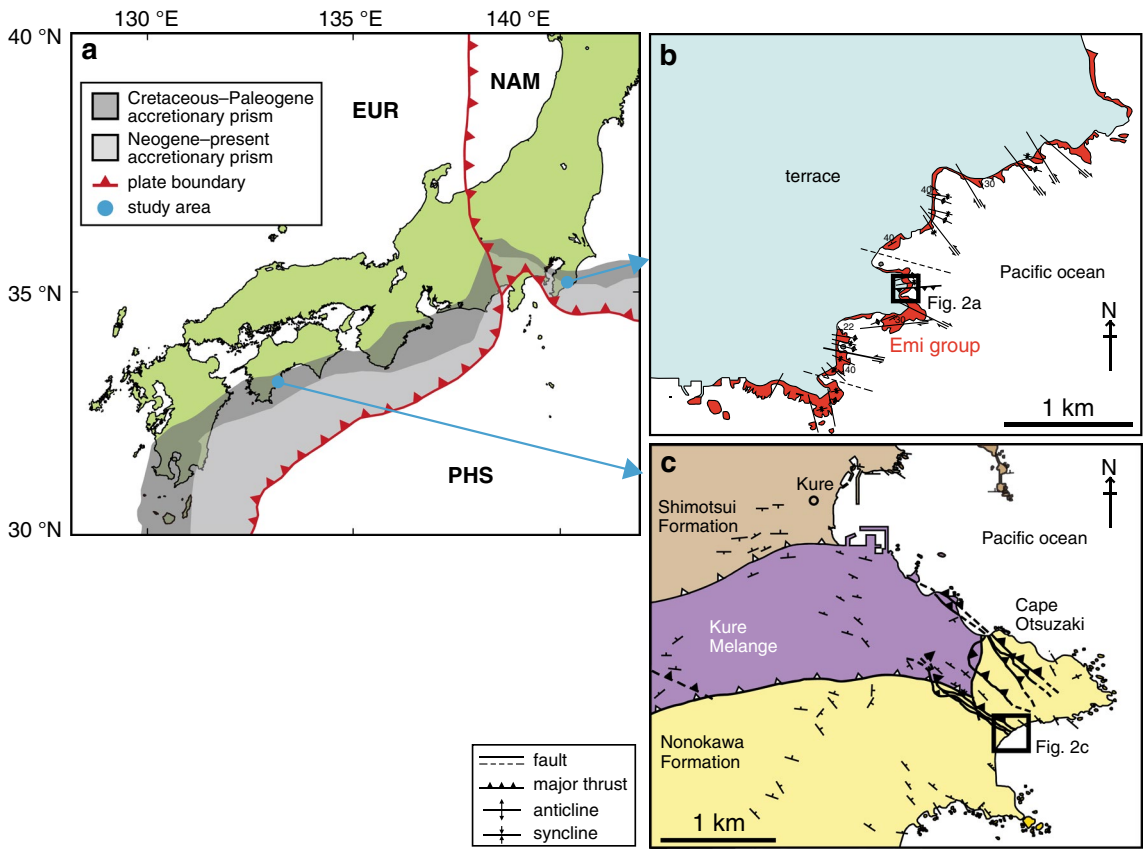

Fig. 1 Location and geology of the studied area. **a** Regional map showing major plate boundaries, the distribution of accretionary complexes of the Japan island arc, and the locations of the two study areas of this paper. *EUR* Eurasia plate, *NAM* North America plate, *PHS* Philippine Sea plate. Maps showing simplified geologic structure in **b** the area of outcrop of the Emi Group, modified from Hirono et al. (2008b), and **c** OSTs around the Kure Mélange, modified from Honda et al. (2011)

measure spectra for both the CM distributed in the thin sections of the slip zones and that extracted from the surrounding host rocks for the heating experiments. The spectra were measured at each point on the target surface with laser spot size of 2 μm and laser power of 0.13 mW. The obtained signal was edge-filtered and dispersed using a 2400 g mm^{-1} grating. For each thin-section sample, spectra were obtained at dozens of target points in areas of similar structure with exposure time of 40 s. For each heated CM sample, spectra were obtained at 25 points with exposure time of 20 s. After a baseline correction for the spectral range 1000–1800 cm^{-1}, to remove fluorescence interference, the areas of the D and G bands were determined using a Lorentzian curve-fitting procedure by using Labspec v. 5.0 software (HORIBA Jobin–Yvon Inc.).

Results

Emi major thrust

A microscopic image of the Emi major thrust sample shows that the fault zone is composed of cataclasite containing three discrete slip zones that form distinct layers of blackish ultracataclasite with clay-size particles (Fig. 3a). The cataclasite contains randomly oriented well-rounded to subrounded lithic fragments of clay to very fine sand size, composed mainly of quartz, plagioclase, K-feldspar, and clasts of older ultracataclasite. The cataclasite shows no indication of melting, such as the presence of fibrous microlite or vesicles, indicating that the maximum temperature of the Emi major thrust has not exceeded 1100 °C (Hamada et al. 2011).

Raman spectra of CM extracted from in and around the slip zones of the Emi major thrust (Fig. 4a–d) show small shoulder peaks at 1200, 1500, and 1620 cm^{-1}, probably corresponding to D4, D3, and D2 bands, respectively, for CM from host rock and cataclasite, but these are absent for ultracataclasite. Both the D and G band peaks (1355 and 1600 cm^{-1}, respectively) of CM from ultracataclasite are distinctly sharper than those of both host rock and cataclasite.

Raman spectra of heated CM from the surrounding rocks in the Emi major thrust show that the D band strengthened with increasing temperature (Fig. 4e). In particular, the intensity of the D band increased markedly at higher temperatures. Small shoulder peaks that were clear in the unheated CM disappeared when the temperature reached 600 °C, and fluorescence interference disappeared at about 800 °C.

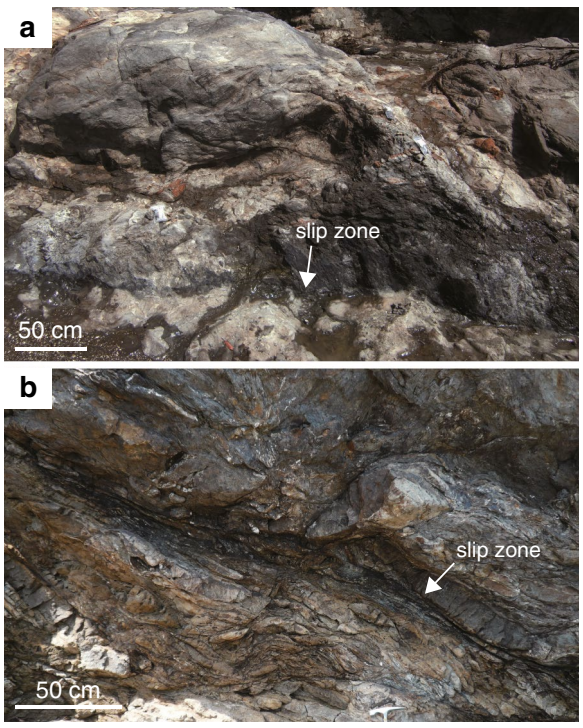

Fig. 2 Outcrop photographs of the deformed zones. **a** A major thrust in the Emi Group. **b** A representative OST within the Kure Mélange. Locations of photographs shown in Fig. 1b, c

Kure OST

Microscopic examination of the fault zone in the Kure OST showed it to be composed of cataclasite and opaque black layers (Fig. 3b). Some of the black layers contain microlites, vesicles, and plagioclase and K-feldspar embayment structures, which indicate that they are in fact pseudotachylyte that experienced melting and therefore temperatures that exceeded 1100 °C (Mukoyoshi et al. 2006). They include opaque particles of CM of several micrometers size and randomly oriented well-rounded to subrounded fragments of quartz, plagioclase, and K-feldspar, also of micrometer size. The cataclasite contains micrograins of quartz, plagioclase, K-feldspar, and older pseudotachylyte. There are also clasts of deformed host rock in the fault zone.

Raman spectra of CM extracted from in and around the slip zone of the Kure OST (Fig. 5a–d) show small shoulder peaks at around 1200, 1500, and 1620 cm^{-1} only for CM from host rock. The G band peaks of CM from cataclasite and pseudotachylyte are sharper and of higher intensity than those from host rock; the D band peak of CM from pseudotachylyte is sharper and of higher high intensity than those of cataclasite and host rock.

Raman spectra of heated CM from surrounding rocks near the Kure OST (Fig. 5e) show that the D band strengthened with increasing temperature and that the D band became markedly stronger at higher temperatures. Small shoulder peaks and fluorescence interference disappeared at around 900 and 1000 °C, respectively.

Discussion

The Raman spectra of CM extracted from ultracataclasite in a slip zone of the Emi major thrust (Fig. 4d) and from pseudotachylyte in a slip zone of the Kure OST (Fig. 5d) are characterized by intense D bands without shoulder peaks. The Raman spectrum of CM from ultracataclasite from the Emi major thrust (Fig. 4d) resembles the spectrum of host-rock CM heated to at least 700 °C (Fig. 4e). That of CM from the pseudotachylyte from the Kure OST (Fig. 5d) resembles the spectrum of host-rock CM heated to 1300 °C (Fig. 5e). To quantify these comparisons, we determined the ratios of the areas under the peaks of the D and G bands (A_D/A_G) (Additional file 1) for all CM spectral analyses from the slip zone and heating experiments.

The A_D/A_G ratio of CM in ultracataclasite from the Emi major thrust (2.06 ± 0.10) was markedly higher than those of CM in the surrounding cataclasite (1.85 ± 0.07) and host rock (1.74 ± 0.13) (colored ranges in Fig. 6a). The A_D/A_G ratio of heated host-rock CM increased from 1.21 ± 0.09 to 2.37 ± 0.21 at temperatures from 300 to 1100 °C, respectively, but then decreased at higher temperatures. The A_D/A_G ratio of CM in ultracataclasite from the Emi major thrust was similar to that of host-rock CM heated to 700 and 1300 °C. Given that a slip zone in the Emi major thrust has not experienced high temperatures of ≥ 1100 °C (Hamada et al. 2011), the most plausible maximum temperature is 700 °C. On the other hand, host-rock CM in the thin section was located at approximately 3 mm away from the ultracataclasite layer (Fig. 3a), and numerical simulation results describing displacement-temperature development at 3 mm away from a slip zone indicate that host-rock CM suffered somewhat high temperature of approximately ≥ 100 °C causing from heat transferred from the slip zone (Additional file 2). Given that the A_D/A_G ratio of CM from the surrounding rocks increased after heating to ≥ 100 °C (Fig. 6a), it is reasonable that the A_D/A_G ratio of host-rock CM in the thin section showed different value of that of intact CM from the surrounding rocks (Fig. 6a).

The A_D/A_G ratio of CM in pseudotachylyte from the Kure OST (2.05 ± 0.09) was markedly higher than those of CM in the surrounding cataclasite (1.94 ± 0.08) and host rock (1.85 ± 0.05) (colored ranges in Fig. 6c). The A_D/A_G ratios of heated host-rock CM increased from 1.80 ± 0.12 to 2.56 ± 0.13 at temperatures from 300 to 1100 °C, but then decreased at higher temperatures. The A_D/A_G ratio of CM in pseudotachylyte from the Kure OST was similar to that of host-rock CM heated to 500–700 and 1300 °C. Taking into consideration the

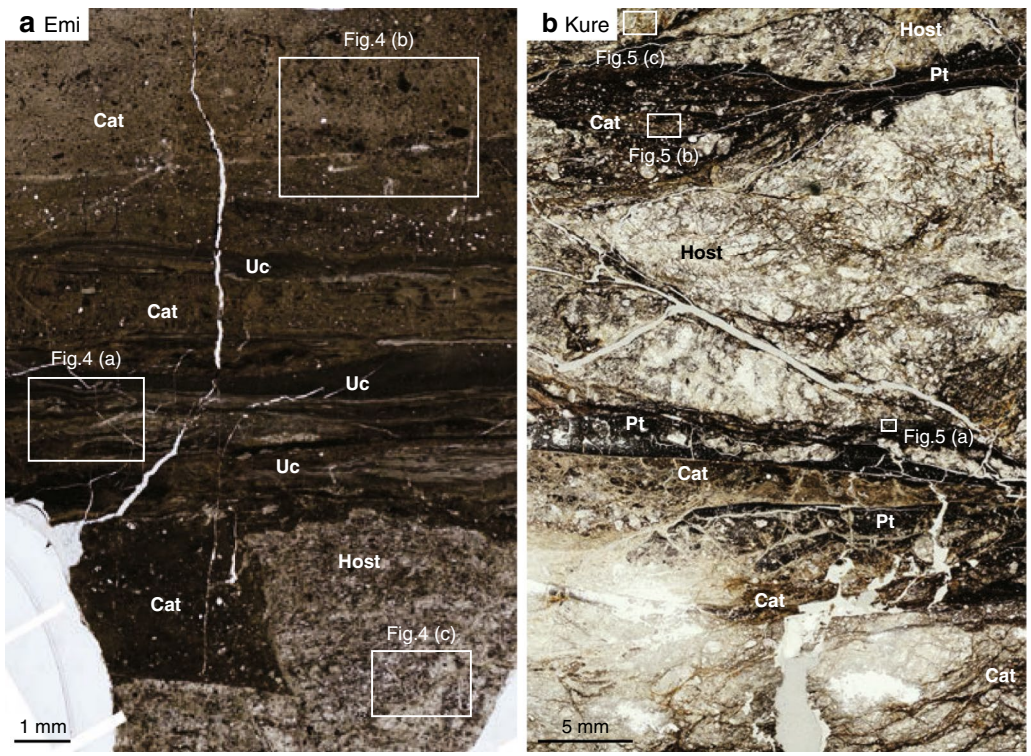

Fig. 3 Photomicrographs showing microstructures in discrete slip zones. **a** The Emi major thrust and **b** the Kure OST. *Uc* ultracataclasite, *Cat* cataclasite, *Host* host rock, *Pt* pseudotachylyte

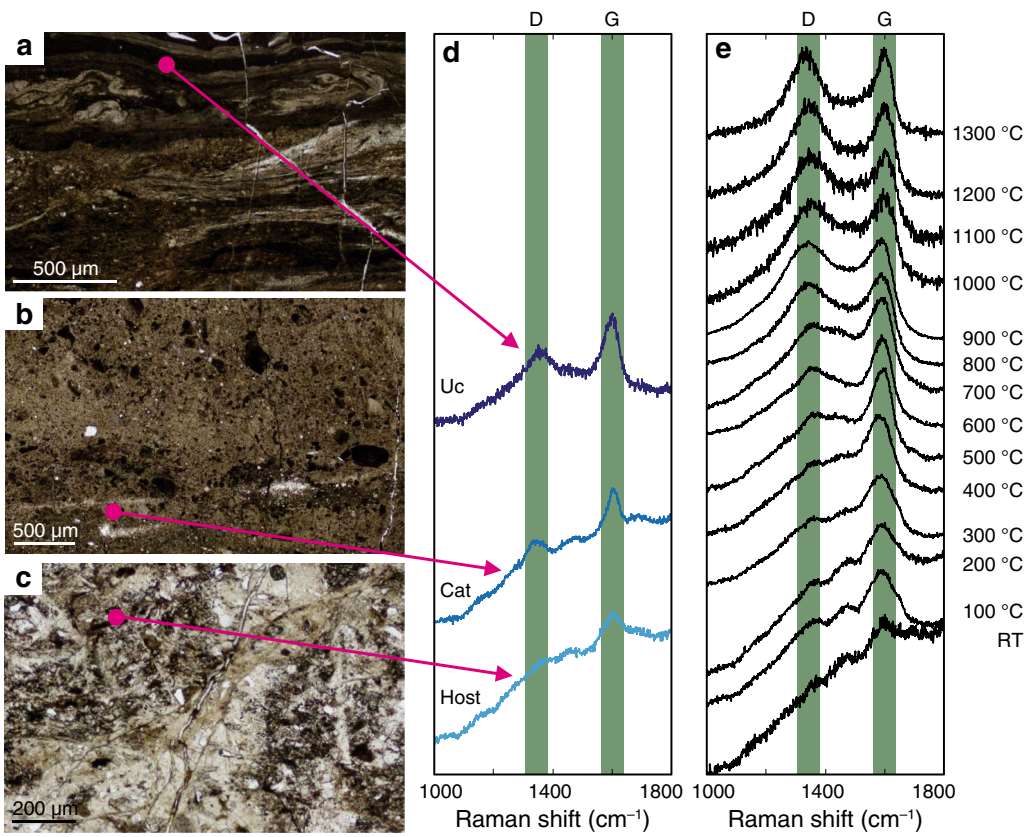

Fig. 4 Locations of CM analytical points (red circles) in the Emi major thrust (see also Fig. 3a). **a** Ultracataclasite, **b** cataclasite, and **c** host rock. **d** Representative Raman spectra of CM samples. **e** Raman spectra of experimentally heated CM extracted from host rock. D, disordered band; G, graphitic band

geological evidence that the maximum temperature of pseudotachylyte reached ≥ 1100 °C (Mukoyoshi et al. 2006), most plausible temperature is 1300 °C for the Kure OST. Thus, the A_D/A_G ratios of the experimentally heated host-rock CM validate our view that CM in ultracataclasite from the Emi major fault and pseudotachylyte from the Kure OST have been heated to temperatures of 700 and 1300 °C, respectively.

The reported range of paleotemperatures in strata of the Emi Group is 50–75 °C (Hirono, 2005), so it is unlikely that a temperature of 700 °C could have been attained without frictional heating during earthquake slip. Temperatures > 350 °C in the Emi major thrust have also been estimated based on fluid-mobile element analysis (Hamada et al. 2011). Similar geochemical analyses of fluid-mobile elements in the Kure OST indicate that the thrust there has also reached temperatures > 350 °C (Honda et al. 2011). Moreover, structural evidence used to define slip-zone material in the Kure OST as pseudotachylyte suggests that friction there might have raised the temperature there to ≥ 1100 °C (Mukoyoshi et al. 2006). However, the above three studies used fault-zone samples that included both cataclasite and fragments of host rock for their geochemical analyses. In contrast, we focused our analyses on discrete and uncontaminated slip zones, which should provide more-reliable estimates of temperatures attained during earthquake slip in the Emi major thrust and the Kure OST.

However, Kitamura et al. (2012) suggested that the commonly used kinetic model for vitrinite reflectance (Sweeney and Burnham 1990) does not yield accurate estimates of the peak temperature in a fault zone because of mechanochemical enhancement of vitrinite maturation. Thus, both a single earthquake accompanied by high frictional heat and multiple slip events at lower temperatures are capable of progressing the maturation of CM (Fulton and Harris 2012). A fast heating rate, several hundreds of degrees Celsius per second during earthquake slip, might delay the reactions. Such mechanochemical activation, cumulative slip events, and fast heating rate might increase the uncertainty of temperatures inferred to have been experienced in the slip zones. However, the quantitative evaluation of their effects on maturation of CM still remains difficult, so we assumed that our

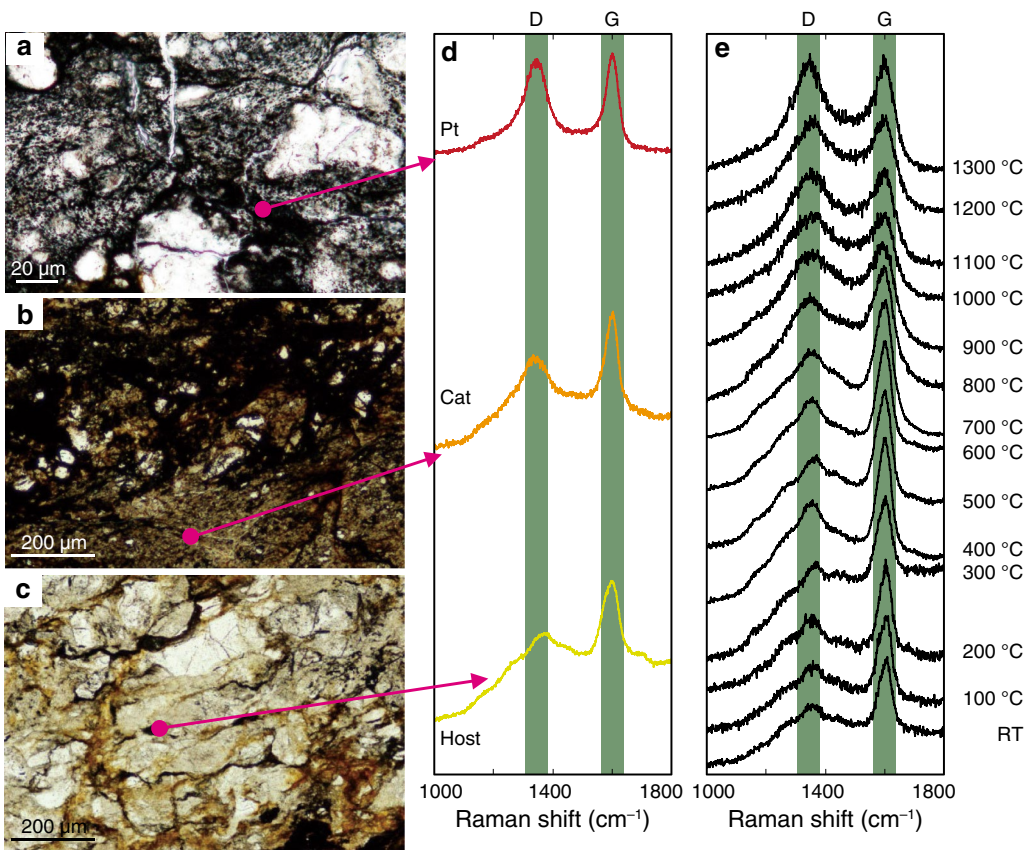

Fig. 5 Locations of CM analytical points (red circles) in the Kure OST (see also Fig. 3b). **a** Pseudotachylyte, **b** cataclasite, and **c** host rock. **d** Representative Raman spectra of CM samples. **e** Raman spectra of experimentally heated CM extracted from host rock. *D* disordered band, *G* graphitic band

estimation of maximum temperature contains uncertainties of ± 100 °C for each fault system.

To examine the slip behavior of the Emi major thrust and Kure OST, we estimated slip parameters (shear stress and slip distance) on the basis of the maximum temperatures recorded in each discrete slip zone. The change in temperature in a slip zone can be expressed by the following one-dimensional heat and thermal diffusion equation:

$$\frac{\partial T}{\partial t} - \frac{\partial}{\partial x}\left(\kappa \frac{\partial T}{\partial x}\right) - \frac{\partial}{\partial t}\left(\frac{\tau D}{wC_p\rho}\right) = 0 \quad (1)$$

where T is temperature, t is elapsed time after the start of slip ($t=0$), κ is thermal diffusivity, x is distance from the center of the slip zone ($x=0$), τ is shear stress, D is slip distance, w is slip-zone thickness, C_p is specific heat capacity, and ρ is rock density. For simplicity, the effects of convective heat transfer, endothermic processes, and dynamic fault weakening are ignored. The time–temperature relationship outside of a slip zone ($w/2 < x$, $-w/2 > x$) can be described as follows:

$$\frac{\partial T}{\partial t} - \frac{\partial}{\partial x}\left(\kappa \frac{\partial T}{\partial x}\right) = 0 \quad (2)$$

Parameters used in the calculation are summarized in Table 1.

If we assume that the stress normal to the fault is equal to hydrostatic stress (i.e., horizontal stress is equal to vertical stress), the amount of frictional heat produced during slip is directly related to the product of the friction coefficient, vertical stress, and slip distance. During earthquake slip, the friction coefficient of the clayey plate-subduction slip zones is commonly 0.1 (e.g., Ujiie and Tsutsumi 2010; Di Toro et al. 2011), so we adopted this value. The burial depths (equivalent to depth to the subducting plate) of the faulted strata of the Emi Group and Kure Mélange have previously been determined to be 1–4 and 2.5–5.5 km, respectively (Mukoyoshi et al. 2006; Hirono et al. 2008b), so we adopted representative depths of 2 and 4 km for the Emi Group and 3 and 5 km for the Kure Mélange. Slip rates during past earthquakes are unknown, so we tested three values (0.1, 0.5, and

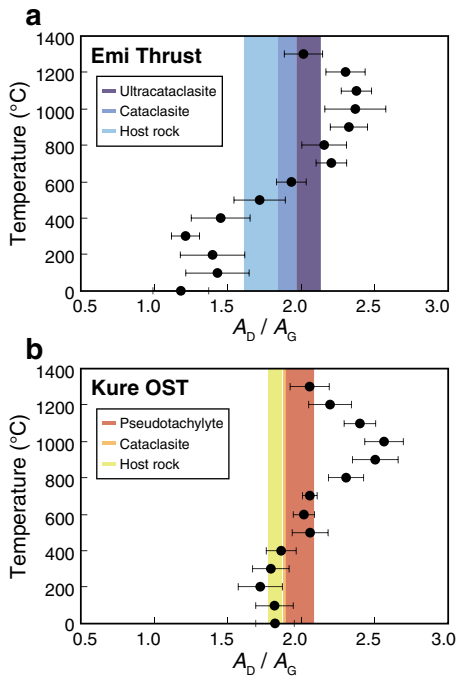

Fig. 6 Temperature dependencies of A_D/A_G ratios of Raman spectra of heated CM from host-rock samples and of CM from discrete slip zones. **a** Emi major thrust; **b** Kure OST

Table 1 Parameters used in calculation of slip distance

Parameter	Emi major thrust	Kure OST
Rock density (kg m^{-3})	2105	1850
Fluid density (kg m^{-3})	1000	1000
Thermal diffusivity (m^2 s^{-1})	3.71×10^{-7}	4.00×10^{-7}
Specific heat capacity (J kg^{-1} K^{-1})	1277	1750
Geothermal gradient (°C km^{-1})	20	50
Seafloor temperature (°C)	4	4
Fault thickness (m)	0.01	0.01

Parameters for the Emi major thrust and the Kure OST are from Hamada et al. (2011) and Kaneki et al. (2016), respectively

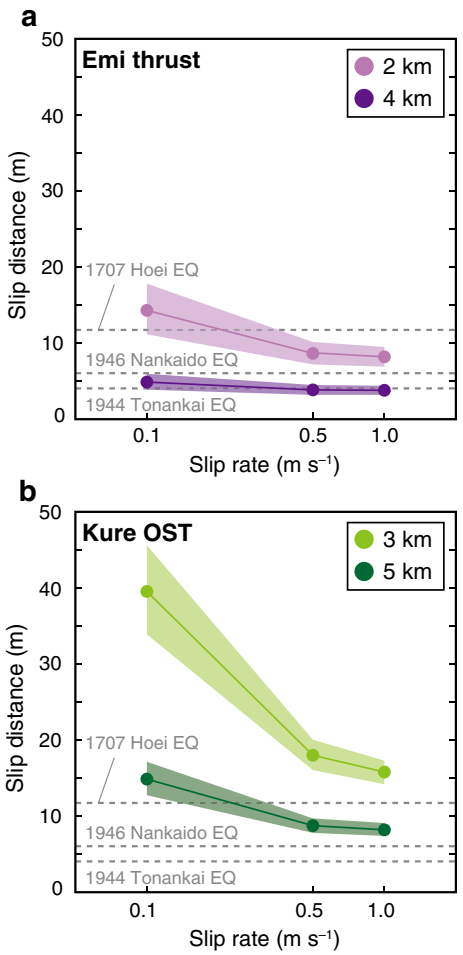

Fig. 7 Results of numerical simulations of heating during fault slip used to determine the amounts of slip necessary to achieve the target temperatures. **a** 700 ± 100 °C in the ultracataclasite layer in the Emi major thrust. **b** 1300 ± 100 °C in the pseudotachylyte layer in the Kure OST for different slip rates and depths of burial. Slip distances during three historical earthquakes are referred from Ando (1975) and Furumura et al. (2011)

1.0 m s^{-1}). By numerically solving Eqs. (1) and (2) using a 0.1 s time increment, a 0.5-mm grid size, and a constant temperature at x = 200 mm as the boundary condition, we obtained the slip distances necessary to achieve temperatures of 600, 700, and 800 °C for the Emi major thrust and 1200, 1300, and 1400 °C for the Kure OST for each combination of depth and slip rate.

The resultant relationships between slip rate and slip distance indicate slip distances of more than 6 and 3 m at depths of 2 and 4 km for the Emi major thrust, respectively (Fig. 7a), and much larger slip distances of more than 14 and 7 m at depths of 3 and 5 km for the Kure OST, respectively (Fig. 7b). In both cases, slip distances were greater for the shallower depth setting, probably because overburden stress was lower at shallower depths. The actual slip rates during past earthquakes are also unknown, but we suggest that the highest slip rate we tested (1 m s^{-1}) is likely closest to the actual slip rate. The resultant slip distances are very consistent with average slip distance during historical Nankai Trough earthquakes such as 1707 Hoei earthquake (Furumura et al. 2011) and 1944 Tonankai and 1946 Nankaido earthquakes (Ando 1975) (Fig. 7).

Conclusions

We performed Raman spectroscopic analyses of CM in thin sections of samples from discrete slip zones in the

Emi major thrust (an ultracataclasite layer) and the Kure OST (a pseudotachylyte layer). Comparison of the A_D/A_G ratios of these Raman spectra with those of experimentally heated CM from nearby host rocks indicated that CM in the ultracataclasite layer from the Emi major thrust had been heated to temperatures up to 700 °C and that CM in the pseudotachylyte layer from the Kure OST had been heated up to 1300 °C. Slip distances for the Emi major thrust and the Kure OST were at least 3 and 7 m, respectively. These slip distances are consistent with those determined from historical records of large tsunamis generated by past Nankai Trough earthquakes (Ando 1975; Furumura et al. 2011). Comparison of the slip distances we determined for the Emi major thrust and Kure OST clearly shows that potential slip distance has regional heterogeneity in major subduction-zone fault systems.

Although our estimates of slip distances did not take into account the influence of kinetics on the maturation of CM, the slip distances we determined probably represent minimum slips for subduction-zone thrusts and thus provide an important contribution to earthquake preparedness plans in coastal areas facing the Nankai and Sagami Troughs.

Additional files

Additional file 1. Peak decomposition method of Raman spectra. Methodology for peak decomposition of the representative Raman spectrum and for calculation of A_D and A_G values.

Additional file 2. Temperature development related to the distance away from a slip zone. Results of numerical simulation showing displacement-temperature development during earthquake at 3 mm away from the slip zone of the Emi major thrust with depth of 2 km and maximum temperature of 700 °C. Other parameters are referred from Table 1.

Authors' contributions

All authors performed the fieldwork. MH carried out the microstructure observations and spectroscopic analyses, SK conducted numerical simulation, and TH carried out heating experiments. All authors wrote the paper. All authors read and approved the final manuscript.

Author details

[1] Department of Geoscience, Interdisciplinary Graduate School of Science and Engineering, Shimane University, Nishikawatsu-cho 1060, Matsue, Shimane 690-8504, Japan. [2] Department of Earth and Space Science, Graduate School of Science, Osaka University, Machikaneyama-cho 1-1, Toyonaka, Osaka 560-0043, Japan.

Acknowledgements

We thank Matt Ikari and one anonymous reviewer for giving many constructive comments, and Associate Editor Phil Cummins for editing this paper. This work was performed as part of a cooperative research program of the Center for Advanced Marine Core Research, Kochi University (Accept 16A053/16B047), and was supported by Grants-in-Aid for Young Scientists (B) (KAKENHI No. 15K21177) and for Scientific Research (B) (KAKENHI No. 15H03737) from the Japan Society for Promotion of Science and by Grants-in-Aid for Scientific Research on Innovative Areas (Crustal Dynamics, KAKENHI No. 26109004) from the Ministry of Education, Culture, Sports, Science and Technology of Japan.

Competing interests

The authors declare that they have no competing interests.

Consent for publication

Not applicable.

Ethics approval and consent to participate

Not applicable.

Publisher's Note

Received: 31 August 2017 Accepted: 26 February 2018
Published online: 08 March 2018

References

Ando M (1975) Source mechanisms and tectonic significance of historical earthquakes along the Nankai Trough, Japan. Tectonophysics 27:119–140. https://doi.org/10.1016/0040-1951(75)90102-X

Baba T, Cummins PR, Hori T, Kaneda Y (2006) High precision slip distribution of the 1944 Tonankai earthquake. Tectonophysics 426:119–134. https://doi.org/10.1016/j.tecto.2006.02.015

Bény-Bassez C, Rouzaud JN (1985) Characterization of carbonaceous materials by correlated electron and optical microscopy and Raman microspectroscopy. Scan Electron Microsc 1:119–132

Beyssac O, Goffé B, Chopin C, Rouzaud JN (2002) Raman spectra of carbonaceous material in metasediments: a new geothermometer. J Metamorph Geol 20:859–871. https://doi.org/10.1046/j.1525-1314.2002.00408.x

Beyssac O, Goffé B, Petitet JP, Froigneux E, Moreau M, Rouzaud JN (2003) On the characterization of disordered and heterogeneous carbonaceous materials by Raman spectroscopy. Spectrochim Acta A 59:2267–2276. https://doi.org/10.1016/S1386-1425(03)00070-2

Chiyonobu S, Yamamoto Y, Saito S (2017) Calcareous nannofossil biostratigraphy and geochronology of Neogene trench-slope cover sediments in the south Boso Peninsula, Central Japan: implications for the development of a shallow accretionary complex. Tectonophysics 710–711:56–68. https://doi.org/10.1016/j.tecto.2016.11.030

Chou YM, Song SR, Aubourg C, Lee TQ, Boullier AM, Song YF, Yeh EC, Kuo LW, Wang CY (2012) An earthquake slip zone is a magnetic recorder. Geology 40:551–554. https://doi.org/10.1130/G32864.1

Di Toro G, Han R, Hirose T, De Paola N, Nielsen S, Mizoguchi K, Ferri F, Cocco M, Shimamoto T (2011) Fault lubrication during earthquakes. Nature 471:494–498. https://doi.org/10.1038/nature09838

Dippel B, Jander H, Heintzenberg J (1999) NIR FT Raman spectroscopic study of flame soot. Phys Chem Chem Phys 1:4707–4712. https://doi.org/10.1039/A904529E

Fujiwara T, Kodaira S, No T, Kaiho Y, Takahashi N, Kaneda Y (2011) The 2011 Tohoku-Oki earthquake: displacement reaching the trench axis. Science 334:1240. https://doi.org/10.1126/science.1211554

Fulton PM, Harris RN (2012) Thermal considerations in inferring frictional heating from vitrinite reflectance and implications for shallow coseismic slip within the Nankai Subduction Zone. Earth Planet Sci Lett 335–336:206–215. https://doi.org/10.1016/j.epsl.2012.04.012

Fulton PM, Brodsky EE, Kano Y, Mori J, Chester F, Ishikawa T, Harris RN, Lin W, Eguchi N, Toczko S, Expedition 343, 343T, KR13-08 Scientists (2013) Low coseismic friction on the Tohoku-Oki fault determined from temperature measurements. Science 342:1214–1217. https://doi.org/10.1126/science.1243641

Furumura T, Imai K, Maeda T (2011) A revised tsunami source model for the 1707 Hoei earthquake and simulation of tsunami inundation of Ryujin Lake, Kyushu, Japan. J Geophys Res 116:B02308. https://doi.org/10.1029/2010JB007918

Guedes A, Valentim B, Prieto AC, Rodrigues S, Noronha F (2010) Micro-Raman spectroscopy of collotelinite, fusinite and macrinite. Int J Coal Geol 83:415–422. https://doi.org/10.1016/j.coal.2010.06.002

Hamada Y, Hirono T, Ishikawa T (2011) Coseismic frictional heating and fluid-rock interaction in a slip zone within a shallow accretionary prism and implications for earthquake slip behavior. J Geophys Res 116:B01302. https://doi.org/10.1029/2010JB007730

Hirono T (2005) The role of dewatering in the progressive deformation of a sandy accretionary wedge: constraints from direct imagings of fluid flow and void structure. Tectonophysics 397:261–280. https://doi.org/10.1016/j.tecto.2004.12.006

Hirono T, Fujimoto K, Yokoyama T, Hamada Y, Tanikawa W, Tadai O, Mishima T, Tanimizu M, Lin W, Soh W, Song SR (2008a) Clay mineral reactions caused by frictional heating during an earthquake: an example from the Taiwan Chelungpu fault. Geophys Res Lett 35:L16303. https://doi.org/10.1029/2008GL034476

Hirono T, Mukoyoshi H, Tanikawa W, Noda H, Mizoguchi K, Shimamoto T (2008b) Frictional behavior and its seismological implications within thrusts in the shallow portion of an accretionary prism. Tectonophysics 456:163–170. https://doi.org/10.1016/j.tecto.2008.04.015

Hirono T, Maekawa Y, Yabuta H (2015) Investigation of the records of earthquake slip in carbonaceous materials from the Taiwan Chelungpu fault by means of infrared and Raman spectroscopies. Geochem Geophys Geosyst 16:1233–1253. https://doi.org/10.1002/2014GC005622

Hirono T, Tsuda K, Tanikawa W, Ampuero JP, Shibazaki B, Kinoshita M, Mori JJ (2016) Near-trench slip potential of megaquakes evaluated from fault properties and conditions. Sci Rep 6:28184. https://doi.org/10.1038/srep28184

Honda G, Ishikawa T, Hirono T, Mukoyoshi H (2011) Geochemical signals for determining the slip–weakening mechanism of an ancient megasplay fault in the Shimanto accretionary complex. Geophys Res Lett 38:L06310. https://doi.org/10.1029/2011GL046722

Ishikawa T, Tanimizu M, Nagaishi K, Matsuoka J, Tadai O, Sakaguchi M, Hirono T, Mishima T, Tanikawa W, Lin W, Kikuta H, Soh W, Song SR (2008) Coseismic fluid–rock interactions at high temperatures in the Chelungpu fault. Nat Geosci 1:679–683. https://doi.org/10.1038/ngeo308

Ito Y, Tsuji T, Osada Y, Kido M, Inazu D, Hayashi Y, Tsushima H, Hino R, Fujimoto H (2011) Frontal wedge deformation near the source region of the 2011 Tohoku-Oki earthquake. Geophys Res Lett 38:L00G05. https://doi.org/10.1029/2011gl048355

Kaneki S, Hirono T, Mukoyoshi H, Sampei Y, Ikehara M (2016) Organochemical characteristics of carbonaceous materials as indicators of heat recorded on an ancient plate-subduction fault. Geochem Geophys Geosyst 17:2855–2868. https://doi.org/10.1002/2016GC006368

Kawai K (1957) Geology of the Kamogawa district, Chiba Prefecture. Jpn Assoc Pet Technol 22:190–197

Kitamura M, Mukoyoshi H, Fulton PM, Hirose T (2012) Coal maturation by frictional heat during rapid fault slip. Geophys Res Lett 39:L16302. https://doi.org/10.1029/2012GL052316

Kodaira S, No T, Nakamura Y, Fujiwara T, Kaiho Y, Miura S, Takahashi N, Kaneda Y, Taira A (2012) Coseismic fault rupture at the trench axis during the 2011 Tohoku-oki earthquake. Nat Geosci 5:646–650. https://doi.org/10.1038/ngeo1547

Kopp H, Kukowski N (2003) Backstop geometry and accretionary mechanics of the Sunda margin. Tectonics 22:1072. https://doi.org/10.1029/2002tc001420

Kuo LW, Song SR, Yeh EC, Chen HF (2009) Clay mineral anomalies in the fault zone of the Chelungpu Fault, Taiwan, and their implications. Geophys Res Lett 36:L18306. https://doi.org/10.1029/2009GL039269

Lachenbruch A, (1986) Simple models for the estimation and measurement of frictional heating by an earthquake. U.S. Geological Survey Open-File Report, 86-508, 13 p

Lahfid A, Beyssac O, Deville E, Negro F, Chopin C, Goffé B (2010) Evolution of the Raman spectrum of carbonaceous material in low-grade metasediments of the Glarus Alps (Switzerland). Terra Nova 22:354–360. https://doi.org/10.1111/j.1365-3121.2010.00956.x

Maekawa Y, Hirono T, Yabuta H, Mukoyoshi H, Kitamura M, Ikehara M, Tanikawa W, Ishikawa T (2014) Estimation of slip parameters associated with frictional heating during the 1999 Taiwan Chi-Chi earthquake by vitrinite reflectance geothermometry. Earth Planets Space 66:28. https://doi.org/10.1186/1880-5981-66-28

Mishima T, Hirono T, Nakamura N, Tanikawa W, Soh W, Song SR (2009) Changes to magnetic minerals caused by frictional heating during the 1999 Taiwan Chi-Chi earthquake. Earth Planets Space 61:797–801. https://doi.org/10.1186/BF03353185

Mitsunashi T, Nasu N, Nirei H (1979) Explanatory text of the geological map of Tokyo Bay and adjacent areas. Geological Survey Japan, 91 pp

Moore GF, Bangs NL, Taira A, Kuramoto S, Pangborn E, Tobin HJ (2007) Three-dimensional splay fault geometry and implications for tsunami generation. Science 318:1128–1131. https://doi.org/10.1126/science.1147195

Mukoyoshi H, Sakaguchi A, Otsuki K, Hirono T, Soh W (2006) Co-seismic frictional melting along an out-of-sequence thrust in the Shimanto accretionary complex. Implications on the tsunamigenic potential of splay faults in modern subduction zones. Earth Planet Sci Lett 245:330–343. https://doi.org/10.1016/j.epsl.2006.02.039

Mukoyoshi H, Hirono T, Hara H, Sekine K, Tsuchiya N, Sakaguchi A, Soh W (2009) Style of fluid flow and deformation in and around an ancient out-of-sequence thrust: an example from the Nobeoka Tectonic Line in the Shimanto accretionary complex, Southwest Japan. Island Arc 18:333–351. https://doi.org/10.1111/j.1440-1738.2009.00670.x

O'Hara K (2004) Paleo-stress estimates on ancient seismogenic faults based on frictional heating of coal. Geophys Res Lett 31:L03601. https://doi.org/10.1029/2003GL018890

Ogawa Y, Ishimaru K (1991) Geologic structures of the Emi Group on the coast of the Emi area southern part of the Boso Peninsula, central Japan. J Geogr (Chigaku Zasshi) 100:530–539

Park JO, Tsuru T, Kodaira S, Cummins PR, Kaneda Y (2002) Splay fault branching along the Nankai subduction zone. Science 297:1157–1160. https://doi.org/10.1126/science.1074111

Plafker G (1972) Alaskan earthquake of 1964 and Chilean earthquake of 1960: implications for arc tectonics. J Geophys Res 77:901–925. https://doi.org/10.1029/JB077i005p00901

Potgieter-Vermaak S, Maledi N, Wagner N, Van Heerden JHP, Van Grieken R, Potgieter JH (2010) Raman spectroscopy for the analysis of coal: a review. J Raman Spectrosc 42:123–129. https://doi.org/10.1002/jrs.2636

Sadezky A, Muckenhuber H, Grothe H, Niessner R, Pöschl U (2005) Raman microspectroscopy of soot and related carbonaceous materials: spectral analysis and structural information. Carbon 43:1731–1742. https://doi.org/10.1016/j.carbon.2005.02.018

Sakaguchi A, Yanagihara A, Ujiie K, Tanaka H, Kameyama M (2007) Thermal maturity of a fold–thrust belt based on vitrinite reflectance analysis in the Western Foothills complex, western Taiwan. Tectonophysics 443:220–232. https://doi.org/10.1016/j.tecto.2007.01.017

Sakaguchi A, Chester F, Curewitz D, Fabbri O, Goldsby D, Kimura G, Li CF, Masaki Y, Screaton EJ, Tsutsumi A, Ujiie K, Yamaguchi A (2011) Seismic slip propagation to the updip end of plate boundary subduction interface faults: vitrinite reflectance geothermometry on Integrated Ocean Drilling Program NanTro SEIZE cores. Geology 39:395–398. https://doi.org/10.1130/G31642.1

Sawamura K, Nakajima T (1980) Miocene silicoflagellate zones in the Boso Peninsula. Bull Geol Surv Jpn 31:333–345

Scholz CH (2002) The mechanics of earthquakes and faulting, 2nd edn. Cambridge University Press, Cambridge

Sun T, Wang K, Fujiwara T, Kodaira S, He J (2017) Large fault slip peaking at trench in the 2011 Tohoku-oki earthquake. Nat Commun 8:14044. https://doi.org/10.1038/ncomms14044

Suzuki Y, Akiba F, Kamiya M (1996) Latest Oligocene siliceous microfossils from Hota Group in southern Boso Peninsula, eastern Honshu, Japan. J Geol Soc Jpn 102:1068–1071

Sweeney JJ, Burnham AK (1990) Evaluation of a simple model of vitrinite reflectance based on chemical kinetics. AAPG Bull 74:1559–1570. https://doi.org/10.1306/0C9B251F-1710-11D7-8645000102C1865D

Tsuji T, Ashi J, Strasser M, Kimura G (2015) Identification of the static backstop and its influence on the evolution of the accretionary prism in the Nankai Trough. Earth Planet Sci Lett 431:15–25. https://doi.org/10.1016/j.epsl.2015.09.011

Tuinstra F, Koenig JL (1970) Raman spectrum of graphite. J Chem Phys 53:1126–1130. https://doi.org/10.1063/1.1674108

Ujiie K, Tsutsumi A (2010) High-velocity frictional properties of clay-rich fault gouge in a megasplay fault zone, Nankai subduction zone. Geophys Res Lett 37:L24310. https://doi.org/10.1029/2010GL046002

Yue H, Lay T (2011) Inversion of high-rate (1 sps) GPS data for rupture process of the 11 March 2011 Tohoku earthquake (Mw 9.1). Geophys. Res. Lett. 38:L00G09. https://doi.org/10.1029/2011gl048700